ARTICLE

Ultraviolet-Initiated *In-Situ* Cross-Linking of Multifunctional Binder Backbones Enables Robust Lithium-Sulfur Batteries

Sha Li [a], Xiao Zhan [a], Gu-Lian Wang [b,*], Hui-Qun Wang [a], Wei-Ming Xiong [a], Li Zhang [a,*]

[a] State Key Laboratory of Physical Chemistry of Solid Surfaces, College of Chemistry and Chemical Engineering, Collaborative Innovation Centre of Chemistry for Energy Materials (iChEM), Tan Kah Kee Innovation Laboratory, Xiamen University, Xiamen, 361005, Fujian, China
[b] Key Laboratory of Colloid and Interface Chemistry, Ministry of Education, School of Chemistry and Chemical Engineering, Shandong University, Jinan, 250100, Shandong, China

Abstract

Lithium-sulfur (Li-S) batteries show attractive prospects owing to their high theoretical energy density, but their commercialization still faces such challenges as lithium polysulfides shuttling, severe volume change and considerable polarization. These stubborn issues place higher demands on each component in the battery, such as the development of multifunctional binders with superior mechanical properties. Herein, ethoxylated trimethylolpropane triacrylate was firstly introduced into sulfur cathodes, and *in-situ* cross-linked by ultraviolet (UV) curing combined with traditional polyvinylidene difluoride binder (*i.e.*, forming a binary binder, denoted as *c*-ETPTA/PVDF) to construct high-loading and durable Li-S batteries. The covalently cross-linked ETPTA framework not only significantly enhances the mechanical strength of the laminate, but also offers a strong chemical affinity for lithium polysulfides due to the abundant oxygen-containing groups. Moreover, the moderate interaction force between ether oxygen bonds and Li^+ further accelerates the Li^+ transport. As such, the S-*c*-ETPTA/PVDF electrode exhibited an ultralow attenuation rate of 0.038% at 2 C over 1000 cycles. Even under a sulfur loading of 7.8 $mg_S \cdot cm^{-2}$, an average areal capacity of 6.2 $mAh \cdot cm^{-2}$ could be achieved after 50 cycles. This work indicates that light-assisted curing technology holds great promise in the fabrication of robust and high-energy-density Li-S batteries.

Keywords: Lithium-sulfur batteries; Ultraviolet curing; *In-situ* cross-linked; Multifunctional binder; High-strength electrode

1. Introduction

Lithium-sulfur (Li-S) batteries are recognized to be one of the most promising next-generation energy storage systems owing to their delightful theoretical specific capacity (1675 $mAh \cdot g^{-1}$), high energy density (2600 $Wh \cdot kg^{-1}$), eco-friendly nature and abundant sulfur resources [1,2]. However, practical implementation of Li-S batteries is still hindered by electrically insulating properties of S_8 and Li_2S_2/Li_2S discharging products, the notorious shuttle effect caused by soluble lithium polysulfide (LiPS) intermediates, and nearly 80% volume fluctuation due to the Li_2S formation during discharge. These daunting challenges severely lead to low sulfur utilization, irreversible capacity fading, and poor electrode structural integrity during cycling [3,4]. Till now, considerable strategies have been adopted to address these issues, *e.g.*, the use of advanced nanotechnology to design polar host materials [5−7], catalytic additives [8,9], functionalized separators [10−12], novel electrolyte additives [13] and solid-state electrolytes [14,15], as well as Li-anode modified engineering [16,17]. However, current methods pay insufficient attention to the structural integrity of the electrodes.

Received 30 July 2022; Received in revised form 13 September 2022; Accepted 4 November 2022
Available online 7 November 2022

* Corresponding author, Gu-Lian Wang, Tel: (86)15706291605, E-mail address: 202120305@mail.sdu.edu.cn.
* Corresponding author, Li Zhang, Tel: (86-592)2882622, E-mail address: zhangli81@xmu.edu.cn.

https://doi.org/10.13208/j.electrochem.2217004

The influence of the volume effect of Li-S batteries is still difficult to overcome during long-term cycling.

As an indispensable component of sulfur cathodes, binders have received less attention, but in recent years, multifunctional binders are increasingly becoming an important strategy to construct durable Li-S batteries. Conventional binders, such as polyvinylidene fluoride (PVDF) and polyvinyl pyrrolidone (PVP) binders, are linear chain polymers with weak LiPSs bonding ability [18]. Apparently, these binders neither alleviate the volume change of the sulfur cathode nor assist in anchoring the soluble intermediates, thus failing to solve the electrode collapse and loss of active materials. In response, researchers designed and ameliorated binders with ample polar functional groups, such as guar gum and xanthan gum, to maintain electrode structural integrity and effectively capture LiPSs [19]. Liu et al. proposed a robust network binder by mixing two polymers together *via* intermolecular interaction of a large number of functional groups in them. Similarly, tannic acid/poly(ethylene oxide) cross-linked hybrid binder was also constructed based on rich hydrogen bond network [20]. Apart from physical cross-linked networks, binders based on chemical cross-linking were also designed and they exhibited the improved mechanical properties. Wang and coworkers disclosed a cross-linked binder of carboxymethylcellulose (CMC) and citric acid (CA) monomers by esterification between the −OH and −COOH groups, which contributed to crack-free and compact electrodes [21]. However, the esterification-based cross-linked networks usually require harsh processing conditions, such as high temperature, protective atmosphere, *etc.* Therefore, mild and more easily scalable chemical cross-linking techniques are highly desirable. *In-situ* ultraviolet (UV)-assisted curing is a promising and low-consumption technology for the preparation of cross-linked polymer [22]. Small molecules or oligomers in the electrodes can be *in-situ* polymerized under UV light irradiation in the presence of a small amount of photo-initiator, which can provide a more uniform and denser network. In this sense, the construction of UV-curable high-strength sulfur cathodes has important application prospects.

Herein, ethoxylated trimethylolpropane triacrylate (ETPTA) is firstly introduced into sulfur cathodes and *in-situ* cross-linked by ultraviolet (UV) curing (forming cross-linked ETPTA, denoted as *c*-ETPTA). The *c*-ETPTA framework can efficiently synergize with traditional polyvinylidene difluoride (PVDF) binder to construct high-loading and durable Li-S batteries. The synthetic process of *c*-ETPTA/PVDF binary binder is illustrated in Scheme 1a, which is cost-effective and can be produced on a large scale. Upon *in-situ* cross-linking, the photo-initiator 2-Hydroxy−2-methyl-propiophenone (HMPP) molecular was excited under UV irradiation to release highly reactive free radicals. The carbon-carbon double bonds (C=C) in ETPTA were then activated and fully polymerized with radicals to form a covalently cross-linked *c*-ETPTA network. The detailed mechanism of UV-initiated polymerization of ETPTA monomer is presented in Scheme 1b. The unique advantages of the *c*-ETPTA/PVDF binary binder are as follows: (i) the *in-situ* strategy enables a more uniform dispersion of the binder components, resulting in a dense and robust network, (ii) the ETPTA component with three ester groups and ether bonds shows high polar property and strongly (de-) complexing ability towards LiPSs, (iii) the moderate interaction force between ether oxygen bonds and Li^+ further accelerates the Li^+ transport. Benefiting from these advantages, sulfur cathodes using *c*-ETPTA/PVDF binder can retain intact morphology even after long-term cycling and exhibit enhanced reaction kinetics. Notably, the S-*c*-ETPTA/PVDF electrode can maintain 61.3% of its original capacity after 1000 cycles at 2 C, concurrently achieving an average Coulombic efficiency over 99.9%. Moreover, the S-*c*-ETPTA/PVDF electrode delivers a superior average areal capacity of 6.2 $mAh \cdot cm^{-2}$ even under a high sulfur loading of 7.8 $mg_S \cdot cm^{-2}$, showing great promise for commercial applications.

2. Results and discussion

2.1. Preparation and characterization of c-ETPTA/PVDF binder

The *in-situ* synthesis of the *c*-ETPTA/PVDF binder was performed directly during the electrode preparation. Firstly, the uniform electrode slurry was cast onto the aluminum foil, and the laminate was cured by exposure to UV light until the ETPTA was fully cross-linked. Fourier-transform infrared (FT-IR) spectrum was recorded to verify the chemical environment of the as-synthesized S-*c*-ETPTA/PVDF electrode. As shown in Fig. 1a, when the as-prepared electrode was not exposed to UV irradiation, a distinct characteristic peak corresponding to C=C vibration peak appeared at 1650 cm^{-1}, and this peak disappeared after the UV curing, indicating that a robust cross-linked *c*-ETPTA network was fully formed [23]. Fig. 1b-c shows the surface morphologies of S-PVDF and S-*c*-ETPTA/PVDF

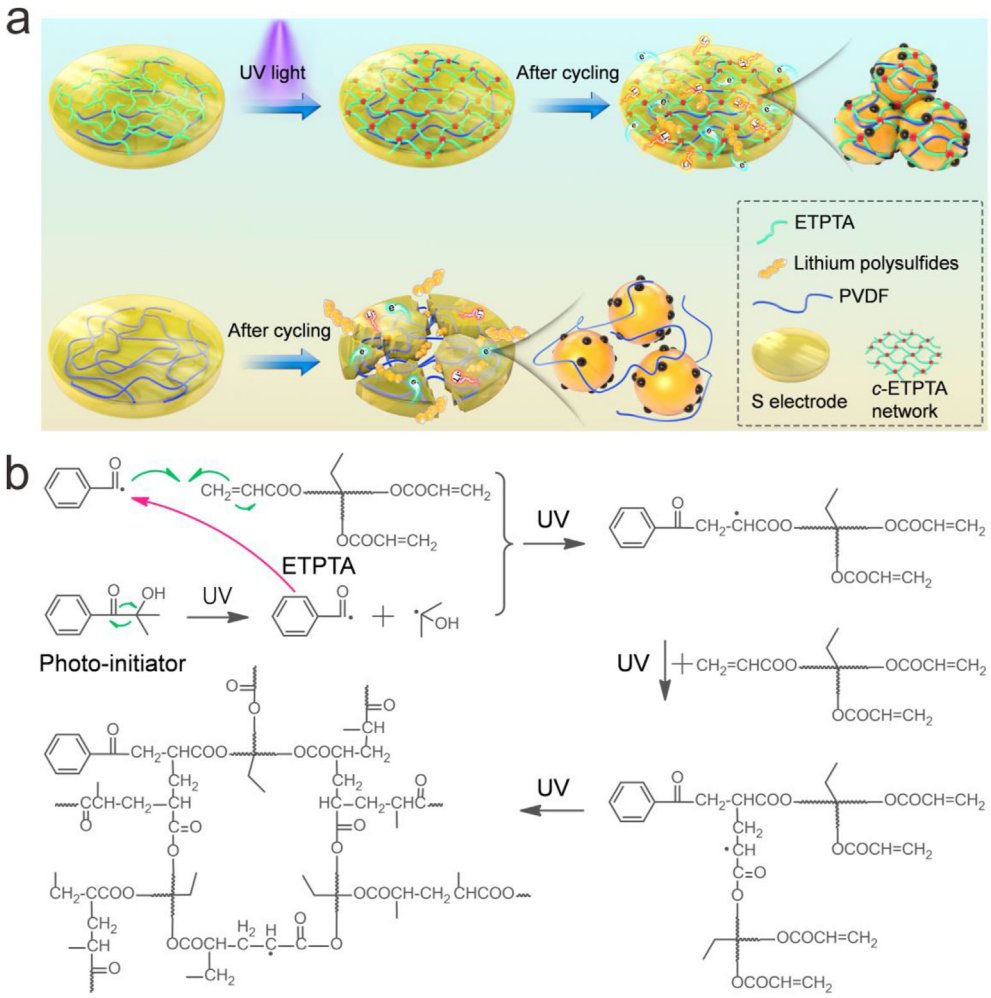

Scheme 1. (a) Schematic illustration of the synthetic process of c-ETPTA/PVDF binary binder and (b) detailed mechanism of UV-initiated in-situ cross-linking of ETPTA.

electrodes. Micron-scale cracks can be observed on S-PVDF electrode, which interrupt the electron transport network and reduce Li^+ conductivity of the entire electrode, resulting in a severer polarization [24]. By contrast, the S-*c*-ETPTA/PVDF electrode shows a seamless structure and uniform distribution of active materials, which is ascribed to a close contact between active materials and conductive agents under the binding of *c*-ETPTA/PVDF binder. The highly compact structure can be confirmed by TEM characterization at larger magnifications (Fig. 1d–e). Moreover, Fig. 1f and S1 display that O, S, F and C elements are distributed homogeneously in the electrode, indicating the consistency of the *in-situ* cross-linking reaction of ETPTA inside the electrode. Strong adhesion between the laminate and the Al collector is vital to achieve advanced Li-S batteries. The peeling off test of S-*c*-ETPTA/PVDF electrode proves closer contact ability between the active materials and the current collectors (Fig. 1g).

Electrolyte permeability of the electrode is another key parameter of the binder. Herein, an electrolyte uptake comparison test was performed in the ether electrolyte. As depicted in Figure S2, the uptake volume of the electrode using *c*-ETPTA/PVDF binder (155%) is slightly lower than that using PVDF binder (164%), validating a more compact and denser electrode structure. Moreover, the electrolyte wetting feature was characterized by contact angle measurements. As displayed in Fig. 1h, the contact angle between the electrolyte and the S-PVDF electrode interface was 10.5°, while the contact angle with the S-*c*-ETPTA/PVDF electrode slightly increased to 17.6°. This small increase is consistent with the compact structure of the S-*c*-ETPTA/PVDF electrode, but apparently does not have any effect on mass transfer. The ability to enhance the adsorption capacity to LiPSs is another important indicator for evaluating Li-S battery binders. A visualized adsorption test was conducted to

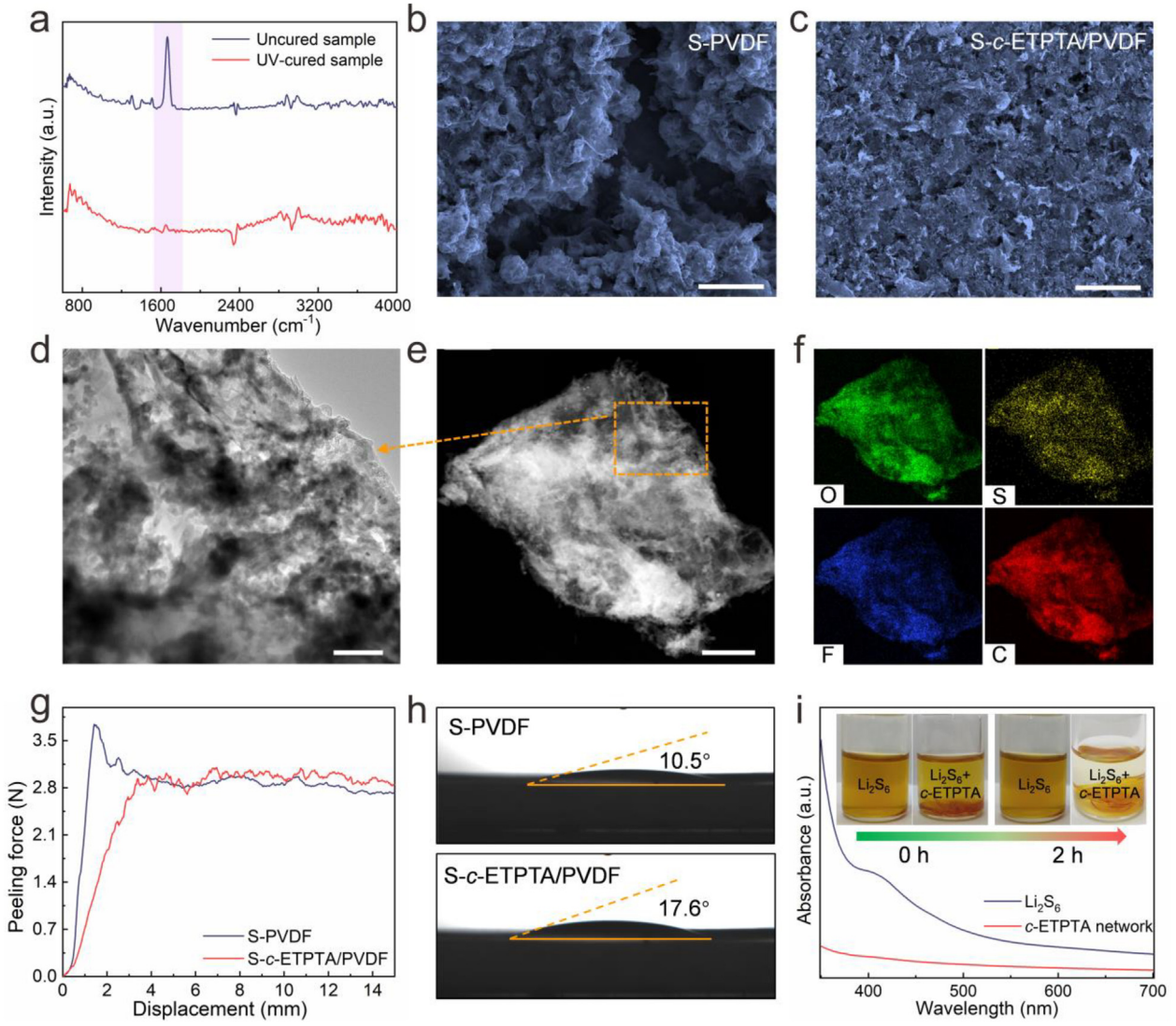

Fig. 1. (a) FT-IR spectra of S-c-ETPTA/PVDF electrodes before and after exposure to UV rays. FESEM images of (b) S-PVDF and (c) S-c-ETPTA/PVDF electrodes. (d, e) TEM images, and (f) corresponding EDS mapping images of highly integrated S-c-ETPTA/PVDF electrode. (g) Peeling off test and (h) contact angle test using organic liquid electrolyte for S-c-ETPTA/PVDF and S-PVDF electrodes. (i) UV−vis adsorption spectra of Li_2S_6 solution before and after adding cured c-ETPTA network. Inset: digital photographs of visualized adsorption test. Scale bar, (b−c) 10 μm, (d) 500 nm, and (e) 2 μm.

estimate the adsorption behaviors of the pristine *c*-ETPTA binder towards soluble polysulfides (inset in Fig. 1i). The addition of *c*-ETPTA membrane to the pure Li_2S_6 solution presents dark yellow. After 2 h, the solution color in the bottle containing the *c*-ETPTA network fades from brownness to nearly colorless, and the reddish brown at the bottom is caused by the discoloration after the adsorption of LiPSs by *c*-ETPTA. Additionally, UV−vis measurement was carried out to test the liquid supernatant. As presented in Fig. 1i, the adsorption signal of Li_2S_6 solution (420 nm) significantly vanishes upon adding the *c*-ETPTA binder [25], demonstrating that the polar *c*-ETPTA binder with abundant ester groups has a stronger affinity for LiPSs. Given the above, the *c*-ETPTA binder shows an excellent dispersion amongst active substances, close contact with Al current collectors, suitable absorptivity of the ether electrolyte, and strong LiPSs trapping ability, which is expected to improve the electrochemical performance of Li-S batteries.

2.2. c-ETPTA/PVDF binder enables durable Li-S batteries

The electrochemical inertness and negligible capacity contribution of the *c*-ETPTA/PVDF binder were verified by cyclic voltammetry (CV) and galvanostatic charge-discharge (GCD) tests (Figure S3). Fig. 2a displays the CV profiles of S-*c*-ETPTA/PVDF and S-PVDF electrodes at a scan rate of

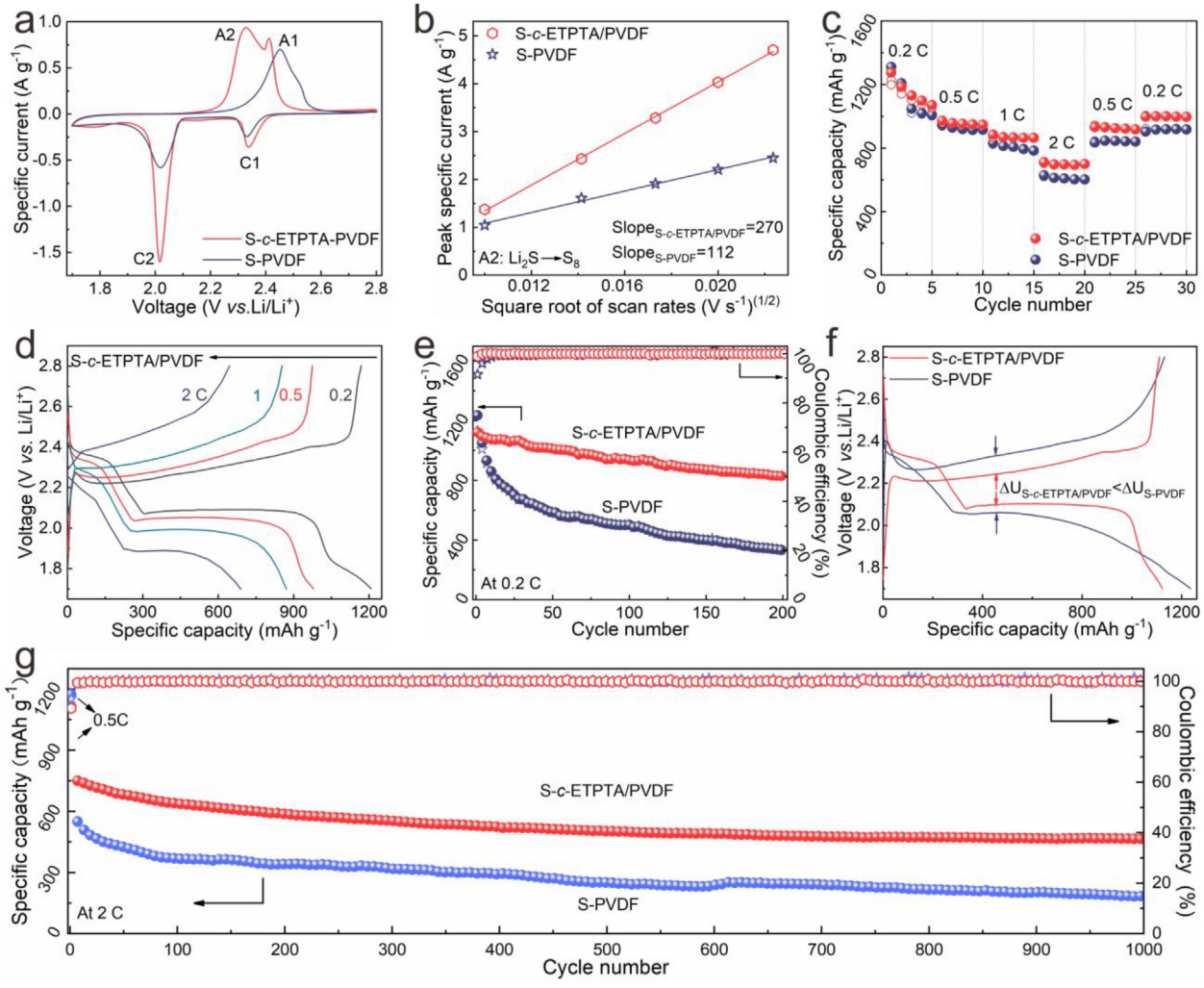

Fig. 2. (a) CV profiles at 0.05 mV·s^{-1}, (b) linear plots of A2 anodic peak currents and (c) rate capabilities under various rates from 0.2 to 2 C of S-c-ETPTA/PVDF and S-PVDF cathodes. (d) Discharge/charge profiles of the S-c-ETPTA/PVDF electrode at various rates. (e) Long-term cycling performance of S-c-ETPTA/PVDF and S-PVDF cathodes at 0.2C and (f) the corresponding initial discharge/charge profiles. (g) Prolonged cycling behaviors of S-c-ETPTA/PVDF and S-PVDF cathodes at 2 C (note: the capacity fluctuation of the S-PVDF electrode around 600th cycle is caused by temperature change).

0.05 mV·s^{-1}. For the S-PVDF electrode, two apparent reduction peaks locate at approximately 2.33 V (labeled as C1) and 2.02 V (labeled as C2), representing the transformation from S_8 to soluble long-chain polysulfides (Li_2Sn, $4 \leq n \leq 8$), and further reduction to solid-state Li_2S_2 or Li_2S [26,27]. During the reverse scan, an anodic peak (labeled as A2) and a broad shoulder peak (labeled as A1) appear at roughly 2.45 V and 2.55 V, respectively, indicating the conversion of Li_2S_2/Li_2S to lithium polysulfide and then to S_8 [28].

As regards the S-*c*-ETPTA/PVDF electrode, the representative two pairs of reduction peaks and oxidation peaks also can be observed, with the increased current response and sharper shape. Meanwhile, as displayed in Figure S5a, the reduction/oxidation peaks of the S-*c*-ETPTA/PVDF electrode obviously shift to higher/lower voltages, implying promoted electrochemical kinetics and alleviated electrochemical polarization. CV measurements at various scan rates from 0.1 to 0.5 mV·s^{-1} were implemented to investigate Li^+ diffusion behaviors of S-*c*-ETPTA/PVDF and S-PVDF electrodes (Figure S5b-c). The linear relationships between the peak currents of the peaks A2, C1, C2 (*I*p) and $v^{1/2}$ are shown in Fig. 2b and S6, indicating a diffusion-controlled reaction. It can be seen that the S-*c*-ETPTA/PVDF electrode shows more rapid Li^+ diffusion behavior than S-PVDF electrode, possibly ascribed to the abundant ether oxygen bonds in the *c*-ETPTA network that facilitate the Li^+ transportation. The corresponding Li^+ diffusion coefficients are listed in Table S1.

Fig. 2c displays the rate capability curves of S-*c*-ETPTA/PVDF and S-PVDF electrodes. For S-*c*-

ETPTA/PVDF electrode, the average specific capacities are 1152, 956, 870 and 699 mAh·g^{-1} at 0.2, 0.5, 1 and 2 C, respectively. When the rate comes back to 0.5 and 0.2 C, the capacity can retain 926 and 998 mAh·g^{-1}, respectively, which presents 96.9% and 86.6% high retention ratios of original capacities, respectively. However, the S-PVDF electrode shows an inferior rate capability, and when the rate recurs to 0.5 and 0.2 C, the capacity can only retain 91.1% and 81.8%, respectively. Markedly, the *c*-ETPTA/PVDF binder is conducive to superior redox stability and good ionic conductivity even under high current rates. The corresponding GCD plots at various rates are depicted in Fig. 2d and S7a, displaying typical discharging and charging plateaus that well agree with the both reduction and oxidation peaks in CV profiles. Figure S7b-c shows capacity contributions at different plateaus, and the larger plateaus capacities of S-*c*-ETPTA/PVDF electrodes demonstrate their higher sulfur utilization. Given the severe shuttling problem of sulfur-based electrodes, especially at low current rates, long-term electrochemical tests at 0.2 C were therefore performed. As Fig. 2e demonstrates, the rapid capacity fading of the S-PVDF electrode can be clearly observed. In stark contrast, the S-*c*-ETPTA/PVDF electrode maintains a high capacity of 800 mAh·g^{-1} even after 200 cycles with an average capacity decay rate of 0.12% per cycle, confirming the strong trapping ability of *c*-ETPTA/PVDF network for soluble LiPSs. Moreover, the corresponding GCD profile of the first cycle is shown in Fig. 2f, the potential difference (ΔU) between the charge and discharge plateaus of the S-*c*-ETPTA/PVDF electrode is obviously smaller than that of S-PVDF electrode. Such lower polarization mainly benefits from the crack-free electrode structure by using robust *c*-ETPTA/PVDF network. In addition, the GCD profiles of the S-*c*-ETPTA/PVDF electrode at various cycles are presented in Figure S8, confirming its stable cycling against LiPSs shuttling. A prolonged cycling test at 2 C was further conducted. As Fig. 2g demonstrates, the capacity of the S-PVDF electrode drops rapidly with an attenuation rate of 0.07% per cycle after 1000 cycles. Note that for the S-*c*-ETPTA/PVDF electrode, this decay rate is significantly reduced to 0.038% per cycle. The excellent cycling behavior of the S-*c*-ETPTA/PVDF electrode is ascribed to the integrated electrode structure supported by the *c*-ETPTA network, rapid ionic transport and ample oxygen-containing functional groups. Table S2 summarizes the cycling performance of Li-S batteries based on various kinds of reported binders in literatures, and the S content (%), electrolyte volume, S loading (mg$_S$·cm^{-2}), *etc.* as main factors are presented, further indicating the superiority of the *c*-ETPTA/PVDF binder.

The self-discharge behavior in Li-S batteries is mainly caused by the severe shuttle effect, leading to the potential drop and capacity attenuation. Herein, the self-discharge behaviors of S-*c*-ETPTA/PVDF and S-PVDF electrodes were investigated (Figure S9). It can be found that when PVDF is used as the binder, the open circuit voltage (OCV) drops more severely than the *c*-ETPTA/PVDF binder. After 160 h, the OCV value of the S-PVDF electrode drops significantly, while the voltage on the S-*c*-ETPTA/PVDF electrode remains stable. This result further demonstrates that the *c*-ETPTA/PVDF binder has efficient LiPSs adsorption capacity and greatly reduces the detrimental shuttling problem.

2.3. Ex situ analysis of the superiority of S-c-ETPTA/PVDF electrode

Electrochemical impedance spectroscopic (EIS) measurements were conducted on the fresh and cycled S-*c*-ETPTA/PVDF and S-PVDF electrodes. As displayed in Fig. 3a, the EIS plots show a depressed semicircle at the high frequency region and an inclined line at the low frequency region before cycling, corresponding to the charge transfer resistance (R_{ct}) and the Warburg coefficient (W_1), respectively [29]. The fitting impedance parameters are shown in Table S3. The S-*c*-ETPTA/PVDF electrode exhibits a lower R_{ct} (66.8 Ω) than the S-PVDF electrode (92.7 Ω), which is attributed to the highly integrated electrode structure. After 50 cycles at 0.2 C, a new interfacial contact resistance (R_{SEI}) at high frequency appears in the EIS plot of cycled S-PVDF electrode, owing to the irreversible formation of Li_2S/Li_2S_2 product [30], and R_{ct} also can be observed at middle frequencies (Fig. 3b). As listed in Table S3, the S-*c*-ETPTA/PVDF electrode exhibits lower R_{SEI} (13.7 Ω) and R_{ct} (9.8 Ω) than the S-PVDF electrode (27.6 Ω and 35.4 Ω). The lower R_{SEI} suggests that less Li_2S/Li_2S_2 is deposited on the electrode interface by using the *c*-ETPTA/PVDF binder. The smaller R_{ct} is attributed to dense cross-linked network and excellent adhesion produced by the *c*-ETPTA/PVDF framework, which maintains electrode structural integrity and forms a continuous and enhanced electron/ion transport network.

The batteries after cycling were disassembled to evaluate the internal situation. FESEM images of cycled cathodes are given in Fig. 3c and d. The S-*c*-ETPTA/PVDF electrode presents a dense morphology even after cycling for 100 times. By

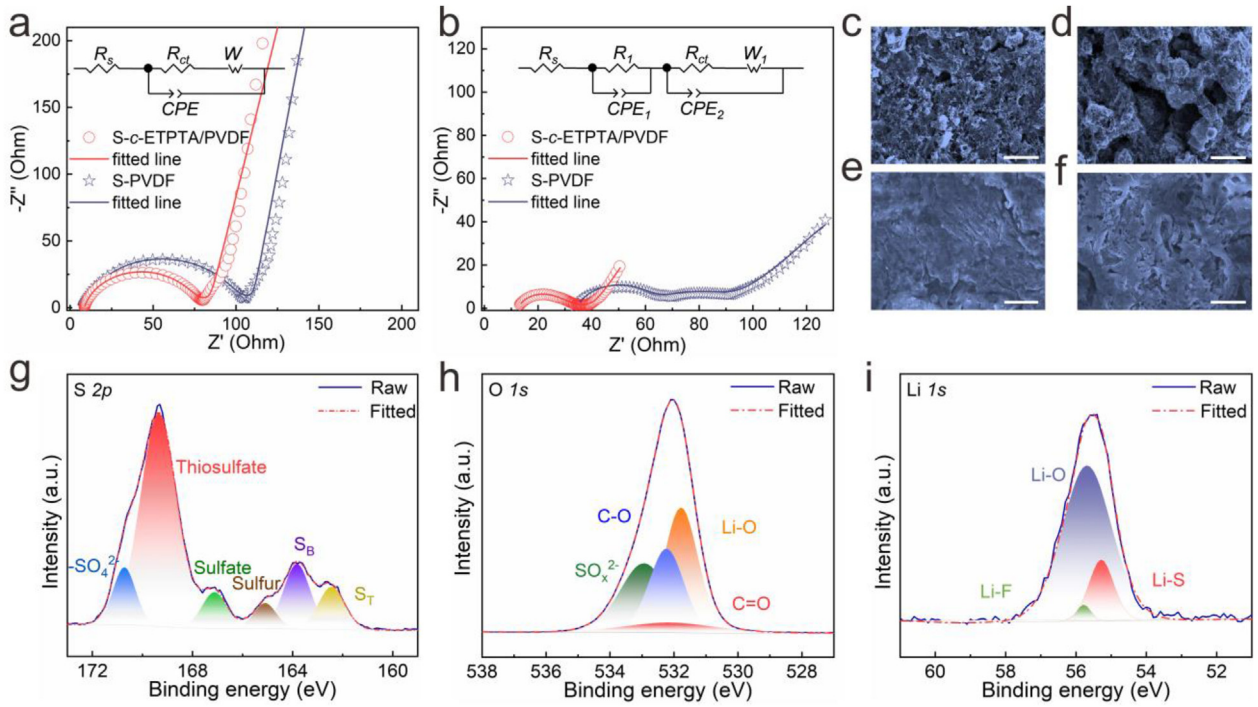

Fig. 3. Nyquist plots of (a) fresh and (b) cycled S-c-ETPTA/PVDF and S-PVDF electrodes. Insets: equivalent circuit diagrams. (c, d) FESEM images of S-c-ETPTA/PVDF and S-PVDF electrodes after 100 cycles. (e, f) FESEM images of the corresponding Li counter anodes after 100 cycles. Deconvoluted XPS spectra of (g) S 2p, (h) O 1s and (i) Li 1s. Scale bar, (c–f) 10 μm.

contrast, the loose S-PVDF electrode displays obvious cracks and holes, resulting in poor adhesion and reduced electronic conductivity. Apparently, the *c*-ETPTA/PVDF network can accommodate volume expansion to maintain the integrity of the electrode structure during cycling. Compared with the traditional PVDF chain binder, the superiority of the *in-situ* cross-linked *c*-ETPTA/PVDF binder is fully demonstrated. The suppressed shuttle effect is also verified by the study of the Li anode surface after 100 cycles. As depicted in Fig. 3e, a relative smooth and intact surface can be observed for Li counter anode by using the S-*c*-ETPTA/PVDF electrode. The *c*-ETPTA/PVDF binder strictly prevents the LiPSs diffusion from penetrating through the PP separator, thus avoiding side reactions on the lithium anode side. By contrast, the Li foil facing S-PVDF electrode is severely corroded (Fig. 3f). Such serious shuttle effect is also reflected from the cycled PP separator in the PVDF-based Li-S cell (Figure S10). Given the above, the *c*-ETPTA/PVDF binder can significantly reduce the active material loss and capacity fading.

X-ray photoelectron spectroscopy (XPS) was employed to further study the interaction between the S-*c*-ETPTA/PVDF electrode and LiPSs. Fig. 3g–i displays the deconvoluted S *2p*, O *1s*, and Li *1s* spectra of the cycled cathode. The S *2p* peaks between 160 and 166 eV are associated with the terminal sulfur S_T (162.3 eV) and bridging sulfur S_B (163.7 eV) of sulfur in polysulfides, indicating that the LiPSs are effectively confined within the S-*c*-ETPTA/PVDF electrode [31]. Stronger peaks located in the 166–172 eV range represent the existences of sulfate and thiosulfate [32].

In the high-resolution O *1s* spectrum, the peak at around 532 eV represents the Li–O chemical bonds existing between the polysulfides and the oxygen-containing groups of the *c*-ETPTA/PVDF binder [33]. In the Li *1s* spectrum, peaks located at 55.2 eV and 55.7 eV are associated with the Li–S and Li–O interactions between LiPSs and the *c*-ETPTA/PVDF binder [34]. The XPS results support the conclusion that the *c*-ETPTA/PVDF binder can greatly handle polysulfides *via* chemical confinement and suppress the shuttle effect, thereby improving the electrochemical behaviors of Li-S batteries.

2.4. c-ETPTA/PVDF binder promotes high-loading Li-S batteries

High sulfur loading and high energy density are driving forces for Li-S battery research. Actually, high-sulfur-loaded electrodes pose great challenges, including increased polarization, limited Li^+ transport, and weakened adhesion between electrode material and current collector, etc. To examine the electrochemical performance under high sulfur loading conditions, S-*c*-ETPTA/PVDF electrodes

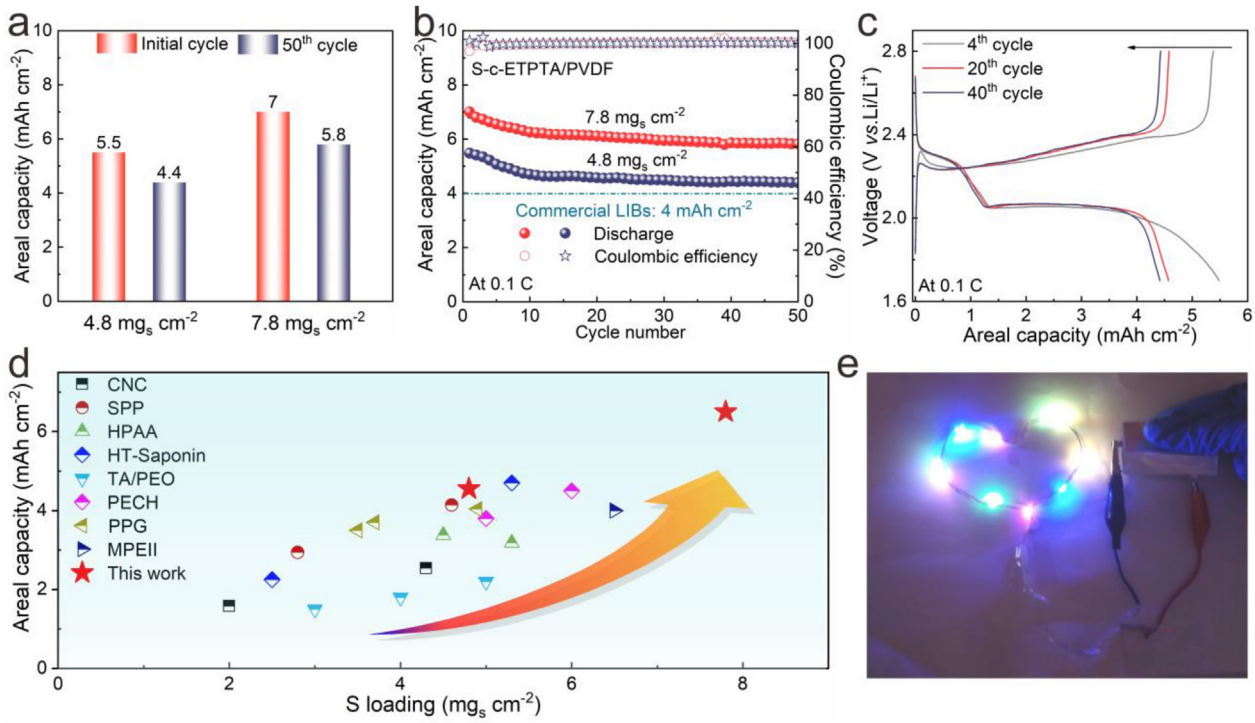

Fig. 4. (a) Areal capacities of S-c-ETPTA/PVDF cathodes with sulfur loadings of 4.8 and 7.8 $mg_S \cdot cm^{-2}$ at the 1st and 50th cycle. (b) Areal capacity and Coulombic efficiency of S-c-ETPTA/PVDF cathodes with sulfur loadings of 4.8 and 7.8 $mg_S \cdot cm^{-2}$ at 0.1C, respectively. (c) Discharge/charge profiles of 4.8 $mg_S \cdot cm^{-2}$ sulfur loading cathodes at various cycles. (d) Comparison of areal capacities of high-loading Li-S batteries using various binders. (e) Digital photograph of LEDs string powered by Li-S pouch cell using c-ETPTA/PVDF binder.

with various loadings have been prepared, and the corresponding thicknesses are shown in Figure S11. When the sulfur loading is 2.8 $mg_S \cdot cm^{-2}$, an initial capacity is close to 1000 $mAh \cdot g^{-1}$ at 0.2 C, and discharge capacity can maintain 70% after 100 cycles (Figure S12). When the sulfur loading is increased to 3.1 $mg_S \cdot cm^{-2}$, a capacity of 900 $mAh \cdot g^{-1}$ can be achieved in the first cycle and a retention rate of 68.6% can be maintained after 100 cycles (Figure S12). When the sulfur loading reaches 4.8 $mg_S \cdot cm^{-2}$, the electrode thickness is about 100 μm (Figure S11c), and its corresponding press density is 0.48 $g \cdot cm^{-3}$. The S-*c*-ETPTA/PVDF electrode shows an initial capacity of *ca*. 5.5 $mAh \cdot cm^{-2}$ at 0.1 C, and 4.4 $mAh \cdot cm^{-2}$ can be maintained after 50 cycles, concurrently achieving an average Coulombic efficiency over 99.8% (Fig. 4a–b). The corresponding GCD profiles with distinct voltage plateaus are presented in Fig. 4c, indicating a low polarization. When the sulfur loading is further increased to 7.8 $mg_S \cdot cm^{-2}$ (Fig. 4a–b), the S-*c*-ETPTA/PVDF electrode can deliver an average areal capacity around 6.2 $mAh \cdot cm^{-2}$ at 0.1 C over 50 cycles. As Fig. 4d demonstrates, *c*-ETPTA/PVDF binder-based Li-S cells show higher areal capacity under high sulfur loading conditions as compared to other binder-based batteries [20,35–41]. Notably, the discharge capacity in our work far exceeds that of commercial LIBs of about 4 $mAh \cdot cm^{-2}$. A soft-package battery is therefore constructed (Figure S13), which can light a string of colored LEDs (Fig. 4e), showing good prospects for its practical application.

3. Conclusions

In summary, a novel *c*-ETPTA/PVDF binder was successfully constructed for durable and high-loading Li-S batteries by *in-situ* UV curing technique. The covalently cross-linked binder network endows the highly integrated sulfur laminate with strong adhesion and exceptional mechanical properties. The abundant ester groups of the *c*-ETPTA/PVDF binder display excellent sieving capability towards LiPSs, which significantly alleviate the severe shuttling effect. Moreover, the moderate interaction force between ether oxygen bonds and Li^+ further accelerates the Li^+ transport. Benefiting from these advantages, the *c*-ETPTA/PVDF binder plays an important role in the preparation of robust and high-energy-density Li-S batteries. The S-*c*-ETPTA/PVDF electrode exhibited an ultralow attenuation rate of 0.038% at 2 C over 1000 cycles. Even under a sulfur loading of 7.8 $mg_S \cdot cm^{-2}$, an average areal capacity of 6.2 $mAh \cdot cm^{-2}$ could be achieved after 50 cycles. This work indicates that light-assisted curing technology holds great promise in the fabrication of robust and high-energy-density Li-S batteries.

The *in-situ* UV-curing method opens up new avenues for the rapid and economical preparation of highly integrated cross-linked electrode structures.

Acknowledgements

The authors acknowledge financial support from the National Natural Science Foundation of China (NSFC, 21875155), the support of National Key Research and Development Program of China (2021YFA1201502), and the support of Nanqiang Young Top-notch Talent Fellowship in Xiamen University.

References

[1] Ji X L, Lee K T, Nazar L F. A highly ordered nanostructured carbon-sulphur cathode for lithium-sulphur batteries[J]. Nat. Mater., 2009, 8(6): 500−506.

[2] Li S, Cen Y, Xiang Q, Aslam M K, Hu B B, Li W, Tang Y, Yu Q, Liu Y P, Chen C G. Vanadium dioxide-reduced graphene oxide binary host as an efficient polysulfide plague for high performance lithium-sulfur batteries[J]. J. Mater. Chem., 2019, 7(4): 1658−1668.

[3] Manthiram A, Fu Y Z, Chung S H, Zu C X, Su Y S. Rechargeable lithium-sulfur batteries[J]. Chem. Rev., 2014, 114(23): 11751−11787.

[4] Zhang L, Qian T, Zhu X Y, Hu Z L, Wang M F, Zhang L Y, Jiang T, Tian J H, Yan C L. *In situ* optical spectroscopy characterization for optimal design of lithium-sulfur batteries[J]. Chem. Soc. Rev., 2019, 48(22): 5432−5453.

[5] Yuan Z, Peng H J, Hou T Z, Huang J Q, Chen C M, Wang D W, Cheng X B, Wei F, Zhang Q. Powering lithium-sulfur battery performance by propelling polysulfide redox at sulfiphilic hosts[J]. Nano Lett., 2016, 16(1): 519−527.

[6] Li S, Xu P, Aslam M K, Chen C G, Rashid A, Wang G L, Zhang L, Mao B W. Propelling polysulfide conversion for high-loading lithium-sulfur batteries through highly sulfiphilic $NiCo_2S_4$ nanotubes[J]. Energy Storage Mater., 2020, 27: 51−60.

[7] Wang N N, Zhang X, Ju Z Y, Yu X W, Wang Y X, Du Y, Bai Z C, Dou S X, Yu G H. Thickness-independent scalable high-performance Li-S batteries with high areal sulfur loading via electron-enriched carbon framework[J]. Nat. Commun., 2021, 12(1): 4519−4528.

[8] Song Y Z, Zhao W, Kong L, Zhang L, Zhu X Y, Shao Y L, Ding F, Zhang Q, Sun J Y, Liu Z F. Synchronous immobilization and conversion of polysulfides on a VO_2-VN binary host targeting high sulfur load Li-S batteries[J]. Energy Environ. Sci., 2018, 11(9): 2620−2630.

[9] Du Z Z, Chen X J, Hu W, Chuang C H, Xie S, Hu A J, Yan W S, Kong X H, Wu X J, Ji H X, Wan L J. Cobalt in nitrogen-doped graphene as single-atom catalyst for high-sulfur content lithium-sulfur batteries[J]. J. Am. Chem. Soc., 2019, 141(9): 3977−3985.

[10] Li Y J, Lin S Y, Wang D D, Gao T T, Song J W, Zhou P, Xu Z K, Yang Z H, Xiao N, Guo S J. Single atom array mimic on ultrathin mof nanosheets boosts the safety and life of lithium-sulfur batteries[J]. Adv. Mater., 2020, 32(8): 1906722−1906731.

[11] Li S, Lin J D, Ding Y, Xu P, Guo X Y, Xiong W M, Wu D Y, Dong Q F, Chen J J, Zhang L. Defects engineering of light-weight metal-organic frameworks-based electrocatalytic membrane for high-loading lithium-sulfur batteries[J]. ACS Nano, 2021, 15(8): 13803−13813.

[12] Xu S N, Zhao T, Wang L L, Huang Y X, Ye Y S, Zhang N X, Feng T, Li L, Wu F, Chen R J. Endoplasmic-reticulum-like catalyst coating on separator to enhance polysulfides conversion for lithium-sulfur batteries[J]. J. Energy Chem., 2022, 67: 423−431.

[13] Fan X X, Yuan R M, Lei J, Lin X D, Xu P, Cui X Y, Cao L, Zheng M S, Dong Q F. Turning soluble polysulfide intermediates back into solid state by a molecule binder in Li-S batteries[J]. ACS Nano, 2020, 14(11): 15884−15893.

[14] Pei F, Dai S Q, Guo B F, Xie H, Zhao C W, Cui J Q, Fang X L, Chen C M, Zheng N F. Titanium-oxo cluster reinforced gel polymer electrolyte enabling lithium-sulfur batteries with high gravimetric energy densities[J]. Energy Environ. Sci., 2021, 14(2): 975−985.

[15] Manthiram A, Yu X W, Wang S F. Lithium battery chemistries enabled by solid-state electrolytes[J]. Nat. Rev. Mater., 2017, 2(4): 16103−16118.

[16] Gu Y, Wang W W, Li Y J, Wu Q H, Tang S, Yan J W, Zheng M S, Wu D Y, Fan C H, Hu W Q, Chen Z B, Fang Y, Zhang Q H, Dong Q F, Mao B W. Designable ultra-smooth ultra-thin solid-electrolyte interphases of three alkali metal anodes[J]. Nat. Commun., 2018, 9: 1339−1347.

[17] Pan H, Zhang M H, Cheng Z, Jiang H Y, Yang J G, Wang P F, He P, Zhou H S. Carbon-free and binder-free Li-Al alloy anode enabling an all-solid-state Li-S battery with high energy and stability[J]. Sci. Adv., 2022, 8(15): 4372−4379.

[18] Seh Z W, Zhang Q F, Li W Y, Zheng G Y, Yao H B, Cui Y. Stable cycling of lithium sulfide cathodes through strong affinity with a bifunctional binder[J]. Chem. Sci., 2013, 4(9): 3673−3677.

[19] Liu J, Galpaya D GD, Yan L J, Sun M H, Lin Z, Yan C, Liang C D, Zhang S Q. Exploiting a robust biopolymer network binder for an ultrahigh-areal-capacity Li-S battery [J]. Energy Environ. Sci., 2017, 10(3): 750−755.

[20] Zhang H, Hu X H, Zhang Y, Wang S Y, Xin F, Chen X D, Yu D S. 3D-crosslinked tannic acid/poly(ethylene oxide) complex as a three-in-one multifunctional binder for high-sulfur-loading and high-stability cathodes in lithium-sulfur batteries[J]. Energy Storage Mater., 2019, 17: 293−299.

[21] Huang X, Luo B, Knibbe R, Hu H, Lyu M Q, Xiao M, Sun D, Wang S C, Wang L Z. An integrated strategy towards enhanced performance of the lithium-sulfur battery and its fading mechanism[J]. Chem. Eur. J., 2018, 24(69): 18544−18550.

[22] Yuan J J, Huang Z, Song Y Z, Li M Y, Fang L F, Zhu B K, Li H Y. *In-situ* crosslinked binder for high-stability S cathodes with greatly enhanced conduction and polysulfides anchoring[J]. Chem. Eng. J., 2021, 426: 128705−128714.

[23] Fan W, Zhang X L, Li C J, Zhao S Y, Wang J. UV-initiated soft-tough multifunctional gel polymer electrolyte achieves stable-cycling Li-Metal battery[J]. ACS Appl. Energy Mater., 2019, 2(6): 4513−4520.

[24] Luo Z, Xu Y, Gong C R, Zheng Y Q, Zhou Z X, Yu L M. An ultraviolet curable silicon/graphite electrode binder for long-cycling lithium ion batteries[J]. J. Power Sources, 2021, 485: 229348−229355.

[25] Ma C, Feng Y M, Liu X J, Yang Y, Zhou L J, Chen L B, Yan C L, Wei W F. Dual-engineered separator for highly robust, all-climate lithium-sulfur batteries[J]. Energy Storage Mater., 2020, 32: 46−54.

[26] Yu Z S, Liu M L, Guo D Y, Wang J H, Chen X, Li J, Jin H L, Yang Z, Chen X A, Wang S. Radially inwardly aligned hierarchical porous carbon for ultra-long-life lithium-sulfur batteries[J]. Angew. Chem. Int. Ed., 2020, 59(16): 6406−6411.

[27] Luo D, Li C J, Zhang Y G, Ma Q Y, Ma C Y, Nie Y H, Li M, Weng X F, Huang R, Zhao Y, Shui L L, Wang X, Chen Z W. Design of quasi-mof nanospheres as a dynamic electrocatalyst toward accelerated sulfur reduction reaction for high-performance lithium-sulfur batteries[J]. Adv. Mater., 2022, 34(2): 2105541−2105550.

[28] Lei J, Fan X X, Liu T, Xu P, Hou Q, Li K, Yuan R M, Zheng M S, Dong Q F, Chen J J. Single-dispersed polyoxometalate clusters embedded on multilayer graphene as a bifunctional electrocatalyst for efficient Li-S batteries[J]. Nat. Commun., 2022, 13(1): 202−211.
[29] Zhang B, Qin X, Li G R, Li G R, Gao X P. Enhancement of long stability of sulfur cathode by encapsulating sulfur into micropores of carbon spheres[J]. Energy Environ. Sci., 2010, 3(10): 1531−1537.
[30] Deng Z F, Zhang Z A, Lai Y Q, Liu J, Li J, Liu Y X. Electrochemical impedance spectroscopy study of a lithium/sulfur battery: modeling and analysis of capacity fading[J]. J. Electrochem. Soc., 2013, 160(4): A553−A558.
[31] Yin Z H, Pan S Y, Cheng Q, Zhang G Z, Yu X Y, Pan Z X, Rao H S, Zhong X H. Mild-method synthesised rGo-TiO_2 as an effective polysulphide-barrier for lithium-sulphur batteries[J]. J. Alloys Compd., 2020, 836: 155341−155349.
[32] Yao S S, Xue S K, Peng S H, Jing M X, Qian X Y, Shen X Q, Li T B, Wang Y H. Synthesis of graphitic carbon nitride at different thermal-pyrolysis temperature of urea and it application in lithium-sulfur batteries[J]. J. Mater. Sci. Mater. Electron., 2018, 29(20): 17921−17930.
[33] Nandasiri M I, Camacho-Forero L E, Schwarz A M, Shutthanandan V, Thevuthasan S, Balbuena P B, Mueller K T, Murugesan V. *In situ* chemical imaging of solid-electrolyte interphase layer evolution in Li-S batteries [J]. Chem. Mater., 2017, 29(11): 4728−4737.
[34] Vorobeva K A, Eliseeva S N, Apraksin R V, Kamenskii M A, Tolstopjatova E G, Kondratiev V V. Improved electrochemical properties of cathode material $LiMn_2O_4$ with conducting polymer binder[J]. J. Alloys Compd., 2018, 766: 33−44.
[35] Chu Y, Chen N, Cui X M, Liu A M, Zhen L, Pan Q M. A multi-functional binder for high loading sulfur cathode [J]. J. Energy Chem., 2020, 46: 99−104.
[36] Wang H, Yang Y, Zheng P T, Wang Y Y, Ng S W, Chen Y K, Deng Y H, Zheng Z J, Wang C Y. Water-based phytic acid-crosslinked supramolecular binders for lithium-sulfur batteries[J]. Chem. Eng. Jpn., 2020, 395: 124981−124991.
[37] Luo X, Lu X B, Chen X D, Chen Y, Yu C Y, Su D W, Wang G X, Cui L F. A functional hyperbranched binder enabling ultra-stable sulfur cathode for high-performance lithium-sulfur battery[J]. J. Energy Chem., 2020, 50: 63−72.
[38] Kim S, Cho M, Lee Y. Saponin-containing multifunctional binder toward superior long-term cycling stability in Li-S batteries[J]. J. Mater. Chem., 2020, 8(20): 10419−10425.
[39] Yang C A, Du Q K, Li Z H, Ling M, Song X Y, Battaglia V, Chen X B, Liu G. *In-situ* covalent bonding of polysulfides with electrode binders in operando for lithium-sulfur batteries[J]. J. Power Sources, 2018, 402: 1−6.
[40] Rashid A, Zhu X Y, Wang G L, Ke C Z, Li S, Sun P F, Hu Z L, Zhang Q B, Zhang L. Highly integrated sulfur cathodes with strong sulfur/high-strength binder interactions enabling durable high-loading lithium-sulfur batteries[J]. J. Energy Chem., 2020, 49: 71−79.
[41] Wang H L, Ling M, Bai Y, Chen S, Yuan Y X, Liu G, Wu C, Wu F. Cationic polymer binder inhibit shuttle effects through electrostatic confinement in lithium sulfur batteries[J]. J. Mater. Chem., 2018, 6(16): 6959−6966.

紫外光引发原位交联多功能粘结剂构筑稳固硫正极

李　莎[a]，湛　孝[a]，王顾莲[b,*]，王慧群[a]，熊伟明[a]，张　力[a,*]
[a]固体表面物理化学国家重点实验室，厦门大学化学化工学院，能源材料化学协同创新中心，嘉庚创新实验室，福建 厦门 361005，中国
[b]山东大学化学与化工学院，胶体与界面化学教育部重点实验室，山东 济南 250100，中国

摘要

锂硫电池因其高理论比容量和高能量密度的独特优势，在下一代储能体系中展现出重要的应用前景。然而，锂硫电池的商业化进程仍面临诸多挑战：如可溶性多硫化锂中间产物造成的“穿梭”问题、充放电过程中体积变化剧烈以及电极硫负载增大时的严重极化等，易导致硫正极的结构坍塌和电化学性能的快速衰变。电池作为一个有机整体，其性能优化是一个系统工程，上述挑战对电池内的每一个组分都提出了更高的要求，例如发展具有更好机械性能的新型粘结剂。在本工作中，我们首次在硫正极中引入乙氧基化三羟甲基丙烷三丙酸酯单体，通过紫外光辅助固化实现原位交联，并与传统聚偏氟乙烯粘结剂构成二元粘结剂（简称 *c*-ETPTA/PVDF），用于制备高强度、高硫负载的长寿命锂硫电池。结果表明，采用共价交联的 *c*-ETPTA/PVDF 粘结剂不但能显著增强电极极片的机械性能，保持循环过程中的结构稳定性，还可借助其丰富的含氧官能团对溶解性多硫化锂中间产物进行高效地捕获。此外，*c*-ETPTA/PVDF 中的醚氧键与锂离子之间适度的相互作用也有助于锂离子的快速输送。因此，S-*c*-ETPTA/PVDF 电极在 2 C 倍率下可稳定循环 1000 次以上，且每个周期的容量衰减率仅为 0.038%。即使当硫面载量提高至 7.8 mg$_S$·cm^{-2} 时，经过 50 个周期循环后，仍可输出 6.2 mAh·cm^{-2} 的高平均放电面容量。本工作展示了紫外光引发原位交联技术在制备稳固的高能量密度锂硫电池方面的巨大应用前景。

关键词：锂硫电池；紫外固化；原位交联；多功能粘结剂；高强度电极